# Self-Test of Air-Coupled Probe for Sensitivity Map Production Using Parabolic Reflector

Linas Svilainis, *Senior Member, IEEE*, Jorge Camacho Sosa Dias, *Member, IEEE*,
Darius Kybartas, *Member, IEEE*, Andrius Chaziachmetovas, *Member, IEEE*,
and Valdas Eidukynas

Abstract—The spatial distribution of a transduction efficiency over the air-coupled probe surface was proposed as a convenient tool for the probe integrity inspection. In this research, a parabolic reflector is used for passive focusing of the acoustic wave on the surface of inspected probe. Therefore, no additional transducer is required for inspection: probe is used for self-inspection. This approach allows to avoid the expensive focused transducer and replaces it by the same-type air-coupled transducers as probe under test. Moreover, the use of the parabolic mirror for focusing is frequency-independent; therefore, such approach allows to inspect a wide range of the probes. Spread spectrum signals were used for excitation to improve the SNR and bandwidth coverage. The results of the experimental measurements of air-coupled transducer sensitivity map with natural and artificial defects implemented have been presented. Comparison with previously proposed techniques is given. It was found that defects presence distorts the focused beam, creating large sidelobes. Therefore, sensitivity map obtained with the proposed technique is lower quality than with previously proposed techniques. Beam profile measurements using a miniature microphone have been presented. Aperture-limiting mask has been proposed to reduce the sidelobes arising due to defects presence and resulting measurements quality has been improved.

Index Terms— Air-coupled ultrasound, aperture mask, beam profile, focused imaging, parabolic on-axis mirror, probe inspection, sensitivity map, spread spectrum signals, transducer defects.
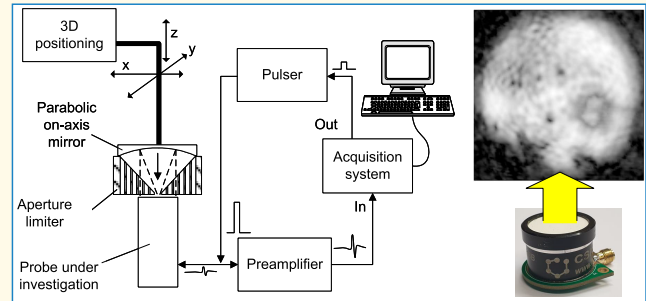
I. Introduction

MAJOR challenge in the air-coupled ultrasound is a large acoustic impedance mismatch between the piezoelement of the transducer and the air [1]. Usual approach to obtain the sensitivity or bandwidth is the application of the multiple matching layers [2], [3], [4], [5]. Many new low impedance matching materials have been proposed [6], [7], [8], [9]. The next challenge is to assemble these materials into multilayer stack: layers are very thin, fragile, usually open-pore, and therefore complex to handle, adjust, and attach [10], [11]. It is also desirable to confirm every layer has uniform

adhesion and thickness over whole probe face. Furthermore, a delamination of layers or electrodes may occur during probe exploitation [12], [13], [14], [15]. The uniformity of the transduction over the whole transducer surface will affect the measurement results [16], [17], [18], [19], [20]. The visual inspection of the probe surface [21] cannot reveal the delamination or local impedance mismatch effects. The evaluation of the electrical impedance or transient response [22], [23] can only detect large, global defects. The measurement of the total (integral of all surface) transduction [24], [25] is not sensitive to the local changes and therefore will not reveal the local deviations. Therefore, it is important to measure the sensitivity map. A method for probe surface sensitivity map measurement was proposed in [26] for immersion probes. Sensitivity map is evaluated using the focused ultrasound beam (higher frequency than inspected probe). Probe surface transmission map can also measured using laser vibrometry [19], [20]. However, the surface of air-coupled probe is fragile and nonreflective; therefore, any coating or reflecting stickers are not possible. It is possible to measure the field at some remote plane and then reconstruct the pressure on the probe's surface by back propagation [18], [27]. However, the available size of the ultrasonic air-coupled microphone [17], [28], [29], [30] limits the attainable resolution; also, complex back-propagation processing is required. Simple solution for the air-coupled probe

Highlights
- **Probe self-evaluation using parabolic on-axis reflector focusing to produce the sensitivity map.**
- **Focal spot has sidelobes if sensitivity is nonuniform over probe surface therefore imaging quality is reduced.**
- **Aperture-limiting mask has been proposed to improve imaging quality.**

inspection was proposed in [31], where similar frequency concave-focused transducers were used. Yet, the application of this method for an air-coupled transducers testing has limitations: 1) complexity to manufacture the wideband concave piezoelectric surface; 2) high near-range sidelobes; 3) the focused air-coupled transducers are expensive; and 4) set of a multiple focused transducers with corresponding frequency range is required for the probes of different frequencies. An attractive alternative was proposed in [26], where off-axis parabolic mirror was used for focusing of the same-type transducer beam on tested probe surface. Lower sidelobes are obtained when the parabolic off-axis mirror is used, and SNR is higher because transmitting and receiving transducers match. Still, a set of transmitting transducers with corresponding frequency range are required.

The novelty of technique proposed here is in the use of an on-axis reflector, using the pulse-echo mode. Then second transducer is not required: probe is in the self-test mode. Reflector is manufactured using 3-D print technology, which reduces the cost of inspection. However, a presence of the far-range sidelobes reduces the quality of sensitivity map. In [31] and [32], the far-range sidelobes were reduced by using the limiting aperture at focal spot. Such approach is not possible in the proposed case because of bidirectional wave propagation. Semi-transparent aperture limiter was proposed to improve the imaging quality. The comparison of the obtained sensitivity map images, obtained using off-axis and on-axis parabolic mirror, is presented.

II. SENSITIVITY MAP MEASUREMENT TECHNIQUES

The idea behind all measurements below is that the focused beam is used for local sensitivity evaluation. The focal spot of the transmitting transducer is positioned on the surface of the tested probe and electrical output signal is assumed to be proportional to local sensitivity at that location. Map is obtained by scanning the focal spot over whole probe's surface. This technique was proposed in [26] and [31]. It uses another (similar or higher frequency) concave-focused transducer to produce a focused beam. However, it is complicated to find focused transducer with matched bandwidth. Additionally, the wideband focused air-coupled transducers are rare, complex to manufacture [1], [33], [34], [35], and also expensive. Composite piezomaterials are used aiming for bandwidth [36], and it is not easy to adhere the composite to the concave surface. Therefore, far-range sidelobes of the focused beam are relatively high. The mainlobe area of the focused beam is small (0.15 mm^2 for 1-MHz frequency and 20 mm element diameter) compared to the probe surface (315 mm^2 at 20 mm diameter, more than 2000 times), which leads to low contrast. A masking aperture was proposed in [31] to solve this issue.
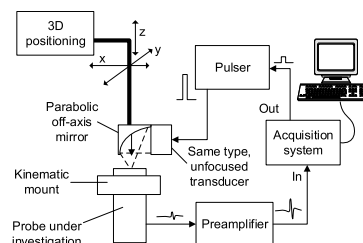

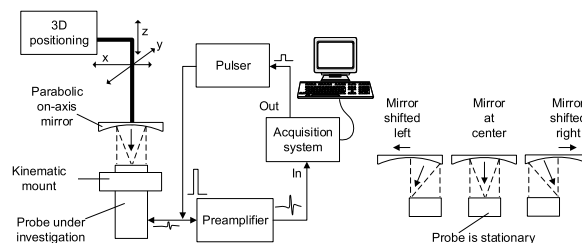Fig. 1. Sensitivity map measurement using parabolic off-axis focusing.

Fig. 2. Proposed sensitivity map measurement using the same transducer and parabolic reflector setup (left) and scanning explanation (right).

A. Using Another Transducer With Parabolic Off-Axis Mirror Focusing

This technique was proposed in [32], and it uses unfocused transmitting transducer. The beam is focused using parabolic off-axis mirror. The setup is presented in Fig. 1.

The transducer of the exactly same type, as inspected probe, can be used, providing perfect bandwidth match. Far-range sidelobes are lower, so the masking aperture is not necessary. Results are better if masking aperture is applied [32]. This setup requires a dedicated mount in order to align the transducer beam with the mirror, and second transducer is still required.

B. Proposed Technique: Using the Same Transducer and Parabolic On-Axis Mirror Focusing

The technique proposed here does not require second transducer, so there is no need of keeping a large set of focused or the same-type transducers just for sensitivity map measurements. An on-axis parabolic mirror is used as a reflector to focus the tested probe unfocused beam back on the surface (Fig. 2, left). Mirror is moved along the x and y plane, shifting the focused beam along the probe's surface (Fig. 2, right).

Parabolic on-axis mirrors are not commercially available, but modern stereolithography (SLA) 3-D printing technology allows for high surface quality and low-cost manufacturing of such reflector. There is no need for additional holder: reflector
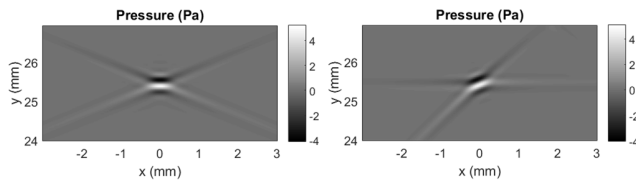
Fig. 3. Zoom-in of the pressure field at the focal spot when probe and mirror axes match (left) and are offset by 10 mm (right).

Fig. 4. Schematic (left) and photograph (right) of the focused beam profile measurement.

can be directly mounted on positioning equipment. From the drawing Fig. 2, it can be concluded that reflector size must be twice the scanning range in order to capture the whole beam.

III. BEAM FOCUSING ANALYSIS

Beam focusing was analyzed by simulation and field measurements.

A. Pressure Field Propagation Study by FEM Simulation for Parabolic On-Axis Mirror

The simulation of ultrasound propagation was carried out first in order to confirm the focusing and investigate the beam behavior at various mirror positions. A finite element method (FEM) simulation using COMSOL 6.1 was carried out in 2-D case (focusing only along the x-axis). Transducer transmission was simulated as ideal pressure plane with 20 mm diameter. Parabolic mirror had a 25.4-mm focal distance. FEM model used 111 712 quartic (fourth order) elements and 56 305 nodes. Maximum element size was 0.02 mm. Time explicit solver was used for modeling the acoustic waves, which was based on a higher order discontinuous Galerkin method with a time-explicit integration scheme. For the time-explicit method used, the governing equations are formulated as a first-order system, in terms of the linearized continuity equation and the linearized momentum equation. The built-in air material model was used in this analysis, so the speed of sound c and the density ρ are defined through the ideal gas law (assuming adiabatic behavior). Transducer transmission was simulated as ideal 20-mm long pressure line. Excitation was applied as Gabor function with 1-MHz center frequency and 60% bandwidth. The parabolic mirror line boundary conditions were set as sound hard boundary, and all other lines of model were set to soft sound boundary.

The results of the focused field for case when mirror and transducer axis match and when mirror axis is offset by 10 mm to the left from transducer axis are presented in Fig. 3.

The field propagation and formation of the focal spot can be studied using the supplementary files ParabFoc_center.avi and ParabFoc_10 mm_offset.avi. It can be noted that focal spot always remains at parabolic mirror axis. The focus is inclined, when reflector and transducer axes are offset, but the size of the focal spot remains approximately the same. The expected focal spot size d at -6 dB [29] can be estimated as follows:

$$d = \frac{1.4\lambda F}{D} = \frac{1.4Fc}{fD}. \tag{1}$$

At frequency $f = 1$ MHz, ultrasound velocity $c = 343$ m/s, piezoelement diameter $D = 20$ mm, and focal distance $F = 25.4$ mm, d is 0.6 mm. It must be noted that it is
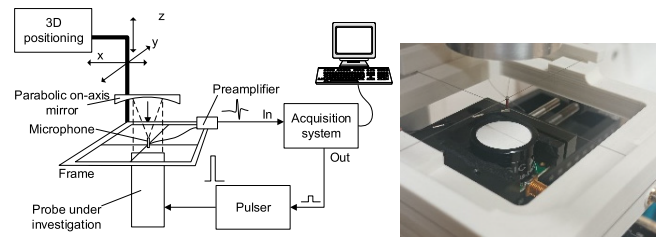
the transducer element diameter D, not the reflector diameter and the wavelength define the focal spot size. Despite it is tempting to reduce the focal distance in order to achieve better resolution, focal distance cannot be smaller than the transducer diameter in order to keep small angle of the rays coming into transducer surface. Otherwise, these rays will be completely reflected from transducer surface and improvement in focal spot size will not be achieved.

The size of the focal spot obtained from FEM simulation was 0.56 mm. Such mismatch can be explained by large edge wave effect due to uniform excitation. Results suggest that sensitivity map can be measured with 0.6-mm resolution. This is more than required for possible defects location. Wavelength in air at 1 MHz is 0.34 mm. The influence of the defect becomes pronounced when it occurs on more than 10% fraction of the transducer surface or is more than several wavelengths. One of the most common defect types is the delamination. Usually, it is much larger than 0.6 mm and results in significant sensitivity drop. Another type of the defects is the lack/loss of the glue. Similar type is the foreign body or air bubble trapped between the layers or inside the matching layer. In such case, defect can be very small, but it will be detected only when its size is more than one wavelength.

B. Focused Beam Measurement by 0.5-mm Ultrasonic Microphone

Parabolic on-axis mirror with focal distance 25.4 mm and diameter 40 mm was manufactured using the SLA 3-D print technology. Field produced by 1-MHz center frequency air-coupled probe (designed and manufactured by the Spanish National Research Council, CSIC, Madrid, Spain [37]) transmitting into on-axis mirror was investigated. Probe had a 20-mm-diameter piezoelement, embedded in aluminum case. Reflector and the probe were mounted on manual x, y, and z positioning and kinematic tilt stages for alignment. Beam at the focal spot was measured using a miniature microphone with 0.5 mm diameter of the sensitive area. The microphone was built using the technique described in [28], connected to 40-dB preamplifier with an input impedance of 5 kΩ and a passband of 90 kHz–3 MHz.

The microphone was hung on two crossing flosses fixed into the rectangular frame (Fig. 4). Frame was attached to a 3-D positioning system.

Microphone was positioned at focal plane and probe was offset from this plane by 10 mm. Probe was excited using the ± 100 V rectangular, 0.75–1.4-MHz frequency, 50-μs duration chirp pulses. The waveform of the excitation signal, registered on transducer input, is presented in Fig. 5, left.
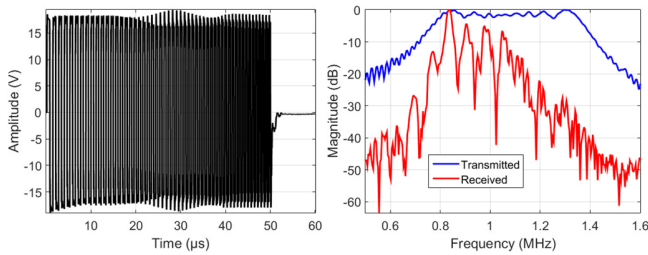
Fig. 5. Excitation signal in time (left) and its spectrum comparison with received by test probe (right).
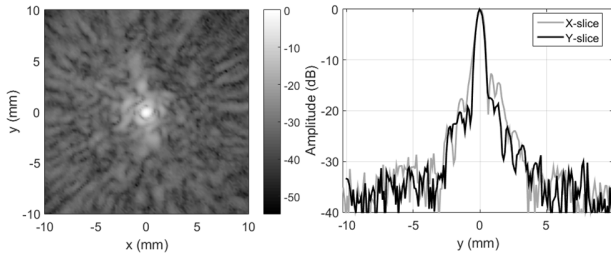

Fig. 6. Measured focused beam profile (left) and cross section (right) for reflector and probe axes aligned over 20 × 20 mm area.
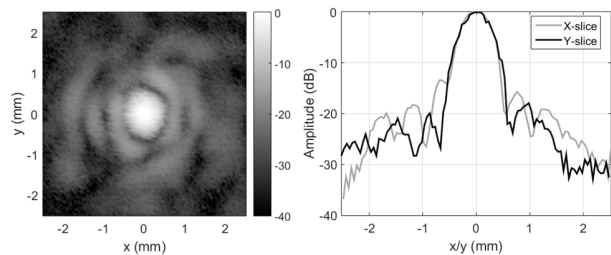

Fig. 7. Measured focused beam profile (left) and cross section (right) for reflector and probe axes aligned over 5 × 5 mm area.

The spectra of the binary sequence used to drive the pulser input are presented in Fig. 5, right as blue curve. The red curve is for signal, received by the ultrasonic microphone. The excitation signal was produced by providing the binary logic level sequences to pulser input. These sequences were stored in buffer memory and clocked out at 100 MHz rate. Signals received were digitized using acquisition system, using 10-bit 100-MHz ADC. The acquired waveforms were filtered using a matched filter. Binary sequence, used to drive the pulser, was used as a reference signal. Both measured and reference signal were transformed into frequency domain. Measured signal was samplewise multiplied with the complex conjugate of the reference signal in the frequency domain. Result was transformed back into the time domain. The cross correlation processing provided pulse compression, so SNR was increased. Peak amplitude of the cross correlation function was used as local sensitivity value. Beam profile was measured using 200 × 200 steps with 100 μm step to cover 20 × 20 mm area and 100 × 100 steps with 50 μm step to cover 5 × 5 mm area. Measured beam profiles when mirror and transducer axes match are presented in Figs. 6 and 7. The gray scale is dB of the peak pressure.

The estimated beam size at −6 dB is 0.74 mm along the x-axis and 0.76 mm along the y-axis. This is close to the

expected 0.6 mm, and expansion is due to 0.5-mm-diameter microphone. It can be seen that far-range sidelobes are approximately −30 dB, while near-range sidelobes are −15 dB.

IV. EXPERIMENTAL SENSITIVITY MAP MEASUREMENT

The measurement of the sensitivity map of the same 1-MHz center frequency air-coupled probe was carried out in order to compare the performance of the off-axis and on-axis focusing influence. Both setups use the same focal distance, 25.4 mm, and the same-type (size) transducer was used in off-axis mirror setup to have the comparable expected resolution. Preamplifier bandwidth was 200 kHz–3 MHz and gain programmable in 7–47 dB range. The input impedance was set to 50 Ω in order to improve the recovery time. The on-axis imaging used Fig. 2 setup, and the off-axis imaging used Fig. 1 setup. Preamplifier had input protection; for Fig. 2, pulser was connected using signal expander in order to ensure pulse-echo mode. For off-axis imaging, optical grade off-axis 90° focus mirror was used (14OAP-1–25-90-AL type from Standa Photonics, Vilnius, Lithuania). Transmitting transducer was mounted in 3-D printed off-axis mirror holder [32]. Excitation used bipolar ±20 V rectangular, 0.75–1.4-MHz frequency, 50-μs duration chirp pulses, produced by bipolar pulser. These sequences were stored in buffer memory and clocked out at 100 MHz rate. Spread spectrum excitation was used to improve the SNR and bandwidth coverage. Sensitivity map was measured using 200 × 200 steps with 100 μm step to cover the 20 × 20 mm area. Signals received were digitized using acquisition system, using 10-bit 100-MHz ADC. The acquired waveforms were filtered using a matched filter. Binary sequence, used to drive the pulser, was used as the reference signal. Both measured and reference signals were transformed into frequency domain. Measured signal was samplewise multiplied with the complex conjugate of the reference signal in the frequency domain. There is an interfering signal, produced by mirror edge in some on-axis imaging cases. Therefore, the pulse compression result was gated before the peak amplitude rectification. The position of the gate was selected using the waveform obtained close to the center at defect-free position. Usually, it was located at $x = 0$ mm and $y = 0$ mm. The peak position of the cross correlation function at this location defined the center of the gate. Gate width was 4 μs. The peak amplitude of the cross correlation function within the gate was used as the sensitivity value.

V. SENSITIVITY MAP OBTAINED BY THE PROPOSED TECHNIQUE: ON-AXIS MIRROR

Three defect arrangements were used with on-axis mirror sensitivity map measurements.
1) Defect free (only natural defects).
2) Strip defect (a 4-mm-wide, 0.1-mm-thick tin strip was placed on the transducer surface).
3) Triangle defect (40-μm-thin copper foil, type 3003310A, Würth Elektronik eiSos GmbH, Waldenburg, Germany, glued on 0.3-mm-thick cardboard placed on the transducer surface).
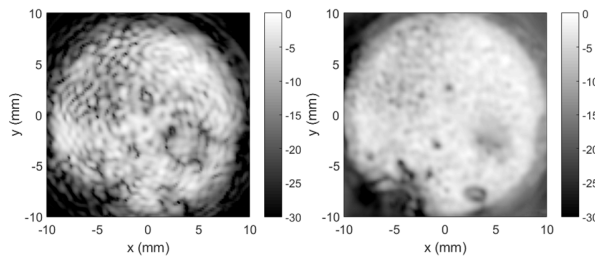
Fig. 8. Sensitivity map obtained using on-axis mirror (left) comparison to off-axis mirror (right) when only natural defects are present.
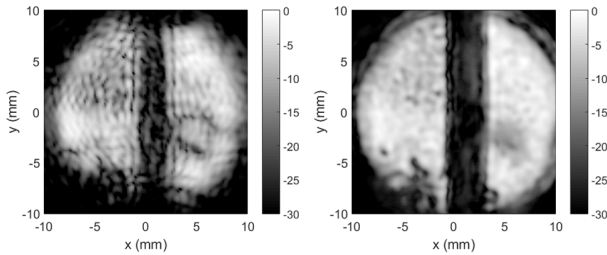

Fig. 10. Sensitivity map obtained using on-axis mirror (left) and off-axis mirror (right) when artificial triangle defect is present.

Fig. 9. Sensitivity map obtained using on-axis mirror (left) and off-axis mirror (right) when artificial strip defect is introduced.

A. Simplified Setup

Two types of on-axis mirrors were used: the SLA-printed plastic and a CNC-manufactured aluminum mirror. Both mirrors had reflecting surfaces polished after manufacturing. Results were the same; therefore, only the results obtained by the plastic mirror are presented in order to indicate that less costly mirror production quality is acceptable.

Sensitivity map measurement results are presented in Fig. 8.

Some natural defects can be seen, which probably have been caused by the air bubbles trapped in the matching layer. The lower left part is probably due to the matching layer delamination. Defects cannot be confirmed by visual inspection, because the surface looks intact. The quality of the on-axis image is significantly different from the off-axis. Ripples appearing on the sensitivity map can be explained by the interference of the focused beam mainlobe and side-lobes. The area covered by the mainlobe is 1000 times smaller than the whole receiving surface. Therefore, even the low-level signals from the sidelobes sum up, reducing the contrast and producing ripples. It was also be noted that the on-axis reflection amplitude is smaller than the one registered with the off-axis mirror. The ratio is approximately 50–30, which corresponds to 4.4 dB. There are two reasons for this difference. According to the results presented in [29], transducer used for transmission in the off-axis setup has 26 dBPa/V transmission sensitivity, but transmitting sensitivity of the probe in on-axis setup is 23 dBPa/V, so there is a 3-dB difference in transmission sensitivity. Remaining 1.4-dB (17%) difference can be assigned to mirror quality or measurement errors.

Results for case when artificial strip defect is introduced are presented in Fig. 9.

It can be noted that the presence of the tin strip reduces the sensitivity by 25 dB. Edges around the defect in case of off-axis mirror are sharp, demonstrating the attainable resolution. It can be noted that the edges of the strip defect are
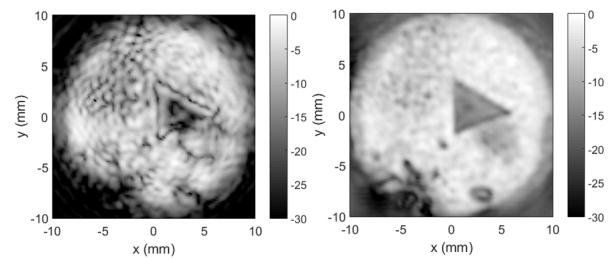
blurred and have ripples around in case of on-axis reflector. Such effect can be expected: transmitting aperture has a slit at the center, which in turn produces significant near-range side-lobes in the focused beam. Then, convolution with such beam produces the edge ripple. Similar situation was encountered in [31]: concave focusing transducer used for imaging was dual-crystal type and therefore had a narrow strip, separating two hemisphere halves. Both sides were used for transmission, but this also created significant sidelobes. In [31], it was proposed to use a limiting aperture, placed at focal spot, which was masking both near and far-range sidelobes. However, such approach is not applicable in the proposed imaging case, since wave has to pass through the focal spot and reflect from the mirror, and only then focal spot is formed.

Results for artificial triangle defect are presented in Fig. 10.

In this case, sensitivity reduction was only 10 dB. Possible reason could be small thickness and adhesion to surface (foil has sticky surface, which was adhered to transducer surface). Lower quality image was produced in case of on-axis mirror: large defect introduced near-range sidelobes, which in turn degraded the measurement quality.

B. Sidelobes Reduction by Using Limiting Aperture

The ripples in sensitivity map are introduced due to different propagation paths. This can be seen by changing the distance between the probe and reflector (see supplementary video Zvar_Clean.mp4). The presence of large defect creates another problem: blurring and edge ripples introduction.

Adding a limiting aperture at the focal spot position [31] is a simple and efficient approach in sidelobes reduction, but cannot be used here, because of the need for two-way wave propagation. However, there is a solution. Field, propagating from probe's surface has flat wavefront in a near field. Honeycomb with thin walls should not disturb this field significantly. Meanwhile, propagation from reflector is mainly inclined and within the cone of focus. Then, it is possible to place a small ring around the focal spot: the honeycomb will hold it in place (see Fig. 11 and supplementary material file ApertureOnMirror.pdf).

Focal spot has enough space to pass through the ring center, which has 2 mm diameter, but the sidelobes, which are offset by 1 mm from center, are blocked. The whole system setup is presented in Fig. 12 and in interactive supplementary file AperturedSystem.pdf.

Aperture effect on the focused beam in case of a strip defect can be seen in Figs. 13–16.

In can be noted that the presence of the large 4-mm-wide strip with reduced sensitivity along the x-axis created large
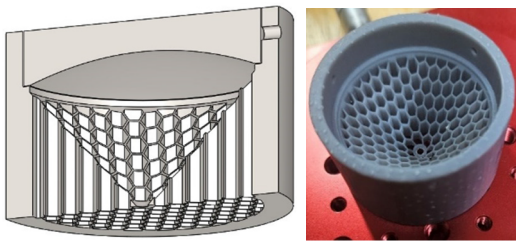
Fig. 11. Proposed masking aperture 3-D drawing and photograph.
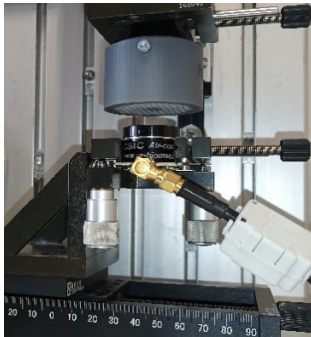

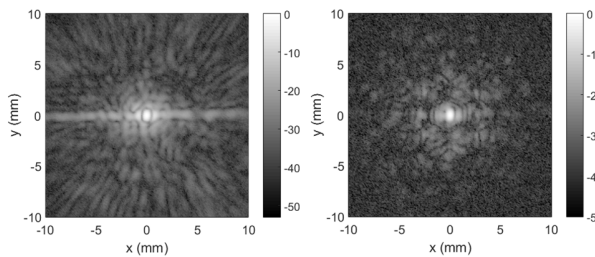Fig. 12. Setup used in measurements when masking aperture is used.

Fig. 13. Original (left) and apertured (right) beam profile comparison over 20 mm range in case of strip defect. Application of the limiting aperture reduces sidelobes.
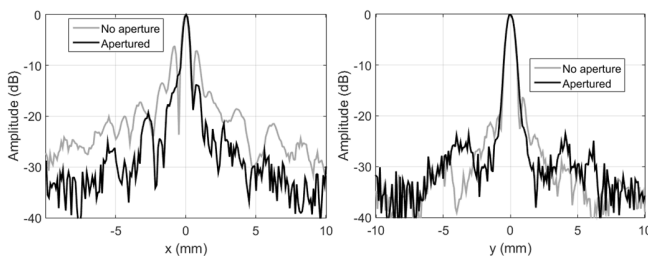

Fig. 14. Original and apertured beam profile cross section comparison over 20 mm range along the x-axis (left) and y-axis (right).
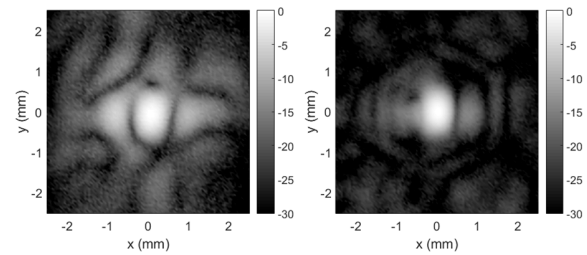

Fig. 15. Original (left) and apertured (right) beam profile comparison over 5 mm range in case of strip defect.
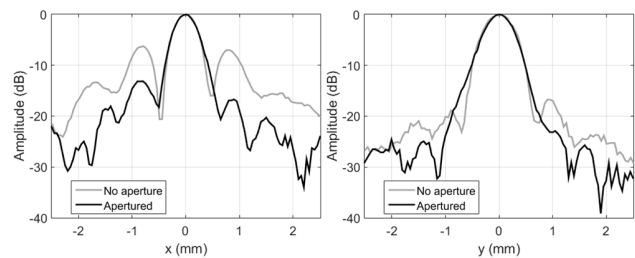

Fig. 16. Original and apertured beam profile cross section comparison over 5 mm range along the x-axis (left) and y-axis (right).
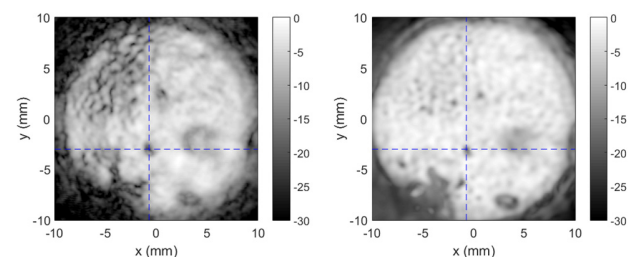

Fig. 17. Comparison of sensitivity maps for apertured on-axis (left) and off-axis (right) imaging in case of only natural defects are present.
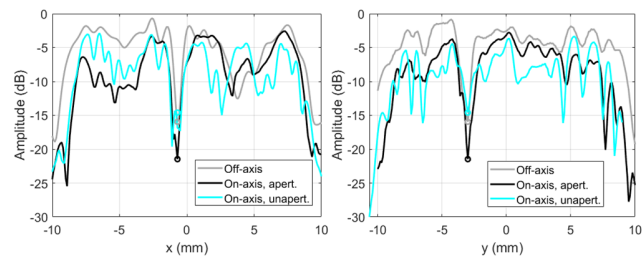

Fig. 18. Comparison of sensitivity map cross section for apertured and unapertured on-axis and off-axis imaging along the x-axis (left) and y-axis (right). Slice over natural defect (marked in Fig. 17).

sidelobes along the y-axis (Fig. 13, left). The application of limiting aperture reduces this sidelobe by approximately 10 dB (Fig. 14, left).

The reduction of the near-range sidelobes can be noted in Figs. 15 and 16. Defect strip is at the center, and this results in effective aperture reduction along the y-axis (Fig. 16, right). Estimated beam size at -6 dB is 0.76 mm along the x-axis and 0.8 mm along the y-axis, which is slightly less than unapertured case.

Positive effect can be noted when such aperture is used for sensitivity map measurement of the defect-free (only natural defects) probe (Fig. 17). Most of the natural defects, like the

dark spot at $x = -0.7$ mm $y = -3$ mm, have better or comparable contrast (see Fig. 18).

The comparison of sensitivity maps when large strip defect is introduced for off-axis and on-axis focusing is presented in Figs. 19 and 20. It can be noted that contrast is lower in case of on-axis focusing: off-axis mirror provides approximately 30 dB, while on-axis reflector case has 25-dB contrast (refer Fig. 20). In addition, the effect of the near-range sidelobes is more pronounced in case of on-axis focusing.

The comparison of sensitivity maps when large triangle defect is introduced is presented in Figs. 21 and 22.
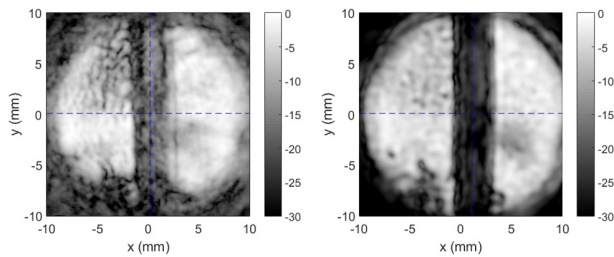
Fig. 19.　Comparison of sensitivity maps for apertured on-axis (left) and off-axis (right) imaging in case of strip defect.
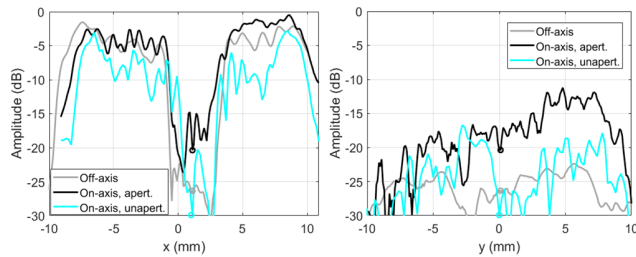

Fig. 20.　Comparison of sensitivity map cross section for apertured and unapertured on-axis and off-axis imaging along the x-axis (left) and y-axis (right). Slice over strip defect (marked in Fig. 19).
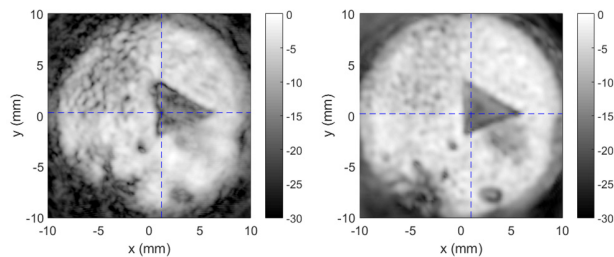

Fig. 21.　Comparison of sensitivity maps for apertured on-axis (left) and off-axis (right) imaging in case of triangle defect.
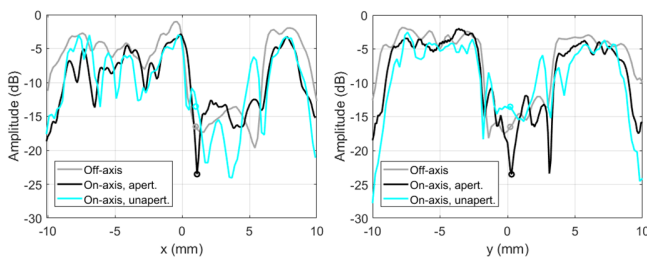

Fig. 22.　Comparison of sensitivity map cross section for apertured and unapertured on-axis and off-axis imaging along the x-axis (left) and y-axis (right). Slice over triangle defect (marked in Fig. 21).

It can be noted that contrast at some spots is even higher, 25 dB, yet image obtained using the off-axis mirror is more homogeneous, though at lower, 20-dB contrast.

C. Performance Evaluation

Several defects were selected for numerical comparison of the results. Nine natural defects (see Fig. 23) were selected, artificial strip and triangle defects.

Defect coordinates were manually selected, and then, rectangular region of interest (ROI) was set around
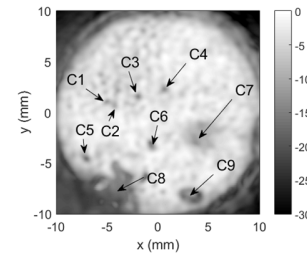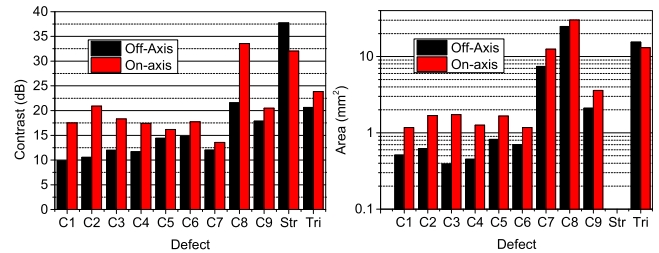

Fig. 23.　Natural defects selected for analysis.

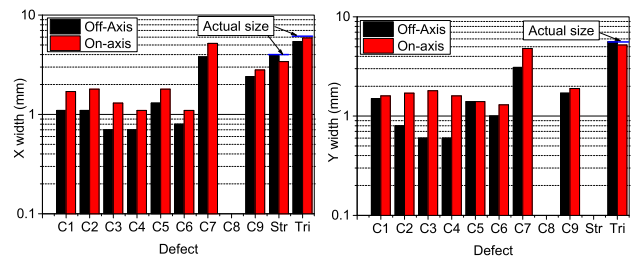Fig. 24.　Comparison of maximum contrast (left) and −6-dB area (right) for on-axis and off-axis imaging.

Fig. 25.　Comparison of defect size along the x-axis (left) and y-axis (right) for on-axis and off-axis imaging.

these coordinates. For small defects ($C1$–$C6$), ROI was 1.8×1.8 mm, large defects ($C7$ and $C8$) used 60×60 mm ROI, and defect 9 used 2.7×2.7 mm ROI. The strip was using 8×20 mm ROI and the triangle: 8.7×8.7 mm. The ratio of the maximum to minimum amplitude within the ROI served as a maximum achievable contrast metrics. The results for achievable contrast are presented in Fig. 24, left.

It can be noted that on-axis imaging achieves better or comparable contrast except strip defect. The defect size was estimated automatically, locating the coordinates with more than −6 dB from maximum within ROI. Estimated defect area for all defect types is presented in Fig. 24, right. Area for strip was not estimated. It can be noted that on-axis imaging overestimates the defect size. The reason is that the application of masking aperture not just reduces the sidelobes but also slightly increases the size of the mainlobe (see Fig. 16).

Defect size along the x and y coordinate is presented in Fig. 25. Blue line indicates actual defect size where it was possible to measure it with caliper. Size for defect $C8$ was not indicated since it has a borderline with piezoelement edge, so estimation results are flawed.

It can be noted that −6 dB sizing produces similar results for on-axis and off-axis measurements. In most of the cases, size obtained using on-axis mirror was slightly larger.

VI. Conclusion

It was demonstrated that transducer sensitivity map can be measured using self-test, when transducer surface is probed by focused beam, produced by a parabolic on-axis mirror. Setup is simple and does not require second transducer (no need for a pool of focused or same type transducers), and only one transducer has to be aligned. The required parts can be printed using SLA technology. Mirror focusing is frequency-independent, which approach allows to inspect the probes of any frequency. Spread spectrum signals were used for excitation to improve the SNR and bandwidth coverage. A 1-MHz center frequency probe was used for performance evaluation of the sensitivity map imaging. In such case, imaging resolution is 0.76 mm.

It was found that the presence of large defect produces near-range sidelobes. Semi-transparent aperture was proposed to reduce the interference ripples and reduce the sidelobes, produced by large defects. Special aperture construction allows the probing signal to pass through but also producing the aperturing effect on the focused beam. A miniature microphone (0.8 mm diameter, 0.5-mm-diameter sensitive area) and holding frame have been built for beam profile measurements. These measurements have confirmed the aperturing effect on the sidelobes. Attainable contrast can reach 30 dB if masking aperture is used.

On-axis reflector is universal: any frequency and size (as long as transducer diameter is less than 40 mm) probes can be inspected. It must be noted that resolution and the contrast will decrease for lower frequency or smaller diameter probes. Therefore, the aperture size has to be increased for probes, where expected beam size according to (1) is larger.

It must be noted that off-axis mirror imaging produces better results, but then, a second transducer of the same type is required. On-axis imaging has another advantage: there are no external active components, and only external reflector has to be added. Therefore, tested probe can remain in a system where it is intended to be used during the evaluation.

Further development is possible applying the techniques previously used on global transducer response (sensitivity, electrical response, and spectral analysis). Previously developed techniques should benefit, because sensitivity map provides information on local response; therefore, defect effect is no longer masked by the response of intact part of the probe.

Sensitivity map should be useful metrics when designing or assembling new transducer. Sensitivity map can be measured at all intermediate assembly procedures to verify the quality of every layer applied.

References

[1] D. E. Chimenti, "Review of air-coupled ultrasonic materials characterization," *Ultrasonics*, vol. 54, no. 7, pp. 1804–1816, Sep. 2014, doi: 10.1016/j.ultras.2014.02.006.

[2] Y.-C. Chen and S. Wu, "Multiple acoustical matching layer design of ultrasonic transducer for medical application," *Jpn. J. Appl. Phys.*, vol. 41, no. 10R, pp. 6098–6107, Oct. 2022, doi: 10.1143/JJAP.41.6098.

[3] T. E. Gomez et al., "Low-impedance and low-loss customized materials for air-coupled piezoelectric transducers," in *Proc. IEEE Ultrason. Symp. Int. Symp.*, vol. 2, Oct. 2001, pp. 1077–1080, doi: 10.1109/ULTSYM.2001.991906.

[4] T. Gudra and D. Banasiak, "Multiparameter analysis of the ultrasonic transducer transfer function using a genetic algorithm," *Appl. Sci.*, vol. 12, no. 11, p. 5325, May 2022, doi: 10.3390/app12115325.

[5] J. Zhou, J. Bai, and Y. Liu, "Fabrication and modeling of matching system for air-coupled transducer," *Micromachines*, vol. 13, no. 5, p. 781, May 2022, doi: 10.3390/mi13050781.

[6] C. M. Kang et al., "Acoustic and rheological characterization of hollow glass microsphere composite for development of optimized air-coupled ultrasonic matching layer," *Ceram. Int.*, vol. 48, no. 21, pp. 32036–32048, Nov. 2022, doi: 10.1016/j.ceramint.2022.07.141.

[7] V. T. Rathod, "A review of acoustic impedance matching techniques for piezoelectric sensors and transducers," *Sensors*, vol. 20, no. 14, p. 4051, Jul. 2020, doi: 10.3390/s20144051.

[8] R. J. Kazys, L. Mazeika, R. Sliteris, and J. Sestoke, "Air-coupled excitation of a slow A_0 mode wave in thin plastic films by an ultrasonic PMN-32%PT array," *Sensors*, vol. 18, no. 9, p. 3156, Sep. 2018, doi: 10.3390/s18093156.

[9] Q. Wu, Q. Chen, G. Lian, X. Wang, X. Song, and X. Zhang, "Investigation of an air-coupled transducer with a closed-cell material matching strategy and an optimization design considering the electrical input impedance," *Ultrasonics*, vol. 115, Aug. 2021, Art. no. 106477, doi: 10.1016/j.ultras.2021.106477.

[10] S. P. Kelly, G. Hayward, and T. E. G. Alvarez-Arenas, "Characterization and assessment of an integrated matching layer for air-coupled ultrasonic applications," *IEEE Trans. Ultrason., Ferroelectr., Freq. Control*, vol. 51, no. 10, pp. 1314–1323, Oct. 2004, doi: 10.1109/TUFFC.2004.1350960.

[11] T. E. G. Alvarez-Arenas, "Acoustic impedance matching of piezoelectric transducers to the air," *IEEE Trans. Ultrason., Ferroelectr., Freq. Control*, vol. 51, no. 5, pp. 624–633, May 2004, doi: 10.1109/TUFFC.2004.1320834.

[12] S. Saffar and A. Abdullah, "Vibration amplitude and induced temperature limitation of high power air-borne ultrasonic transducers," *Ultrasonics*, vol. 54, no. 1, pp. 168–176, Jan. 2014, doi: 10.1016/j.ultras.2013.04.008.

[13] W. Ding, M. Bavencoffe, and M. Lethiecq, "Modeling and experimental characterization of bonding delaminations in single-element ultrasonic transducer," *Materials*, vol. 14, no. 9, p. 2269, Apr. 2021, doi: 10.3390/ma14092269.

[14] M. S. Z. Dehabadi and M. Jahed, "Compensation for electrical fatigue in piezoelectric transducers," *IEEE Trans. Instrum. Meas.*, vol. 72, 2023, Art. no. 6503711, doi: 10.1109/TIM.2023.3284939.

[15] W. Ding, M. Bavencoffe, and M. Lethiecq, "Health monitoring of single-element piezoelectric transducer using its electromechanical admittance," *IEEE Trans. Ultrason., Ferroelectr., Freq. Control*, vol. 68, no. 5, pp. 1819–1827, May 2021, doi: 10.1109/TUFFC.2020.3047944.

[16] M. S. Z. Dehabadi and M. Jahed, "Fault detection of piezoelectric array element using acoustic field and particle swarm optimization," in *Proc. 29th Nat. 7th Int. Iranian Conf. Biomed. Eng. (ICBME)*, Dec. 2022, pp. 282–286, doi: 10.1109/ICBME57741.2022.10052990.

[17] G. Benny, G. Hayward, and R. Chapman, "Beam profile measurements and simulations for ultrasonic transducers operating in air," *J. Acoust. Soc. Amer.*, vol. 107, no. 4, pp. 2089–2100, Apr. 2000, doi: 10.1121/1.428491.

[18] S. J. Sanabria, T. Marhenke, R. Furrer, and J. Neuenschwander, "Calculation of volumetric sound field of pulsed air-coupled ultrasound transducers based on single-plane measurements," *IEEE Trans. Ultrason., Ferroelectr., Freq. Control*, vol. 65, no. 1, pp. 72–84, Jan. 2018, doi: 10.1109/TUFFC.2017.2773619.

[19] L. Hu et al., "Calculation of acoustic field based on laser-measured vibration velocities on ultrasonic transducer surface," *Meas. Sci. Technol.*, vol. 29, no. 5, May 2018, Art. no. 055001, doi: 10.1088/1361-6501/aaaafb.

[20] P. Pietroni and G. M. Revel, "Development of a methodology for the Characterisation of air-coupled ultrasound probes," in *Proc. 9th Int. Conf. Vib. Meas. Laser Noncontact Techn.*, vol. 1253, 2010, pp. 106–115, doi: 10.1063/1.3455447.

[21] *Non-Destructive Testing—Characterization and Verification of Ultrasonic Examination Equipment—Part 2: Probes*, Standard EN 12668-2:2010, 2010.

[22] X. Peng, N. Zhao, C. Xu, L. Hu, and X. Fu, "Frequency-dependent equivalent modelling of broadband air-coupled transducers," *Meas. Sci. Technol.*, vol. 31, no. 2, Feb. 2020, Art. no. 025110, doi: 10.1088/1361-6501/ab49f1.

[23] A. Habib, A. Shelke, U. Amjad, U. Pietsch, and S. Banerjee, "Nonlocal damage mechanics for quantification of health for piezoelectric sensor," *Appl. Sci.*, vol. 8, no. 9, p. 1683, Sep. 2018, doi: 10.3390/app8091683.

[24] X. Li, Z. Dai, G. Zhang, S. Zhang, and H. Jeong, "Determining the responsivity of air-coupled piezoelectric transducers using a comparative method: Theory and experiments," *IEEE Trans. Ultrason., Ferroelectr., Freq. Control*, vol. 68, no. 10, pp. 3114–3125, Oct. 2021, doi: 10.1109/TUFFC.2021.3084756.

[25] G. M. Revel, G. Pandarese, and A. Cavuto, "The development of a shock-tube based characterization technique for air-coupled ultrasonic probes," *Ultrasonics*, vol. 54, no. 6, pp. 1545–1552, Aug. 2014, doi: 10.1016/j.ultras.2014.04.010.

[26] L. Svilainis, D. Kybartas, A. Aleksandrovas, and T. E. G Alvarez-Arenas, "High frequency focused imaging for ultrasonic probe integrity inspection," *NDT & E Int.*, vol. 116, Dec. 2020, Art. no. 102360, doi: 10.1016/j.ndteint.2020.102360.

[27] T. Marhenke et al., "Air-coupled ultrasound time reversal (ACU-TR) for subwavelength nondestructive imaging," *IEEE Trans. Ultrason., Ferroelectr., Freq. Control*, vol. 67, no. 3, pp. 651–663, Mar. 2020, doi: 10.1109/TUFFC.2019.2951312.

[28] L. Svilainis, A. Chaziachmetovas, V. Eidukynas, T. G. Álvarez-Arenas, and S. Dixon, "Miniature ferroelectret microphone design and performance evaluation using laser excitation," *IEEE Trans. Ultrason., Ferroelectr., Freq. Control*, vol. 69, no. 12, pp. 3392–3401, Dec. 2022, doi: 10.1109/TUFFC.2022.3220082.

[29] L. Svilainis, A. Chaziachmetovas, P. Kaskonas, and T. E. Gomez Alvarez-Arenas, "Ultrasonic needle hydrophone calibration in air by a parabolic off-axis mirror focused beam using three-transducer reciprocity," *Ultrasonics*, vol. 133, Aug. 2023, Art. no. 107025, doi: 10.1016/j.ultras.2023.107025.

[30] E. Vatankhah, Y. Q. Meng, Z. H. Liu, X. Y. Niu, and N. A. Hall, "Characterization of high intensity progressive ultrasound beams in air at 300 kHz," *J. Acoust. Soc. Amer.*, vol. 153, no. 5, pp. 2878–2886, May 2023, doi: 10.1121/10.0019376.

[31] L. Svilainis, A. Chaziachmetovas, D. Kybartas, and T. Gomez Alvarez-Arenas, "Air-coupled ultrasonic probe integrity test using a focused transducer with similar frequency and limited aperture for contrast enhancement," *Sensors*, vol. 20, no. 24, p. 7196, Dec. 2020, doi: 10.3390/s20247196.

[32] L. Svilainis, A. Chaziachmetovas, A. Aleksandrovas, D. Kybartas, and T. G. Alvarez-Arenas, "Air coupled probe integrity test using same type probe on parabolic mirror," in *Proc. IEEE Int. Ultrason. Symp. (IUS)*, Oct. 2022, pp. 1–4, doi: 10.1109/IUS54386.2022.9958231.

[33] X. Y. Wang, H. D. Wu, X. D. Zhang, D. Zhang, X. Gong, and D. Zhang, "Investigation of a multi-element focused air-coupled transducer," *AIP Adv.*, vol. 8, no. 9, Sep. 2018, Art. no. 095010, doi: 10.1063/1.5045698.

[34] D. A. Hutchins, T. J. Robertson, and D. R. Billson, "New designs of focused air-coupled ultrasonic transducer," *Revista de Acustica*, vol. 33, pp. 3–4, Jan. 2002.

[35] T. E. G. Alvarez-Arenas, J. Camacho, and C. Fritsch, "Passive focusing techniques for piezoelectric air-coupled ultrasonic transducers," *Ultrasonics*, vol. 67, pp. 85–93, Apr. 2016, doi: 10.1016/j.ultras.2016.01.001.

[36] R. Kazys, L. Mazeika, R. Sliteris, and A. Voleisis, "Online profiling of nonplanar objects by high-resolution air-coupled ultrasonic distance measurements," *IEEE Trans. Instrum. Meas.*, vol. 56, no. 5, pp. 1825–1830, Oct. 2007, doi: 10.1109/TIM.2007.903627.

[37] T. E. Gomez Alvarez-Arenas, "Air-coupled piezoelectric transducers with active polypropylene foam matching layers," *Sensors*, vol. 13, no. 5, pp. 5996–6013, May 2013, doi: 10.3390/s130505996.

Jorge Camacho Sosa Dias (Member, IEEE) was born in Montevideo, Uruguay, in 1979. He received the B.S. degree in electronic engineering from the Universidad de la República, Montevideo, in 2004, and the Ph.D. degree from the Universidad Complutense de Madrid, Madrid, Spain, in 2010.

He is currently a Tenured Scientist with the Spanish National Research Council (CSIC), Institute of Physical and Information Technologies, Madrid. His work is focused on the field of applied acoustics, in particular, and on advanced real-time ultrasonic imaging methods and technologies.

Darius Kybartas (Member, IEEE) received the Ph.D. degree from Kaunas University of Technology, Kaunas, Lithuania, in 2004.

Since 2011, he has been an Associate Professor with the Department of Electronics Engineering, Kaunas University of Technology. His current research interests include high-frequency electronics, radio wave propagation, and ultrasound.

Andrius Chaziachmetovas (Member, IEEE) received the Ph.D. degree from Kaunas University of Technology, Kaunas, Lithuania, in 2007.

Since 2009, he has been an Associate Professor with the Department of Electronics Engineering, Kaunas University of Technology. His current research interests include ultrasonic measurements, ultrasound electronics, high-voltage pulsers, software development, embedded systems, and time of flight estimation.

Linas Svilainis (Senior Member, IEEE) received the Ph.D. degree from Kaunas University of Technology, Kaunas, Lithuania, in 1996.

Since 2009, he is a Full Time Professor at the Department of Electronics Engineering, Kaunas University of Technology, where he is currently a Principal Investigator with the Signal Technologies Group. He has worked in the area of ultrasonics for more than 30 years and has authored three books, more than 150 articles, and holds two patents. His current areas of research are design and optimization of ultrasound electronics, ultrasonic signal processing, time delay (time-of-flight, ToF) estimation, spread spectrum signals, air-coupled ultrasound, large-scale LED video displays, electromagnetic compatibility, and EMI protection of electronic systems.

Dr. Svilainis is an Associate Editor of IEEE TRANSACTIONS ON INSTRUMENTATION AND MEASUREMENT journal.

Valdas Eidukynas received the Ph.D. degree from Kaunas University of Technology, Kaunas, Lithuania, in 1996.

Since 2019, he is a Full Time Professor at the Department of Mechanical Engineering and Design, Kaunas University of Technology. His current research interests are computer-aided modeling and numerical analysis methods and tools in static and dynamic analysis of solid bodies and fluid–structure interaction under the static, dynamic, seismic, and thermal loading as acoustic and elastic waves propagation in various materials as well multiphysics analysis including piezo effects.